REPORT 1096

EXPERIMENTAL DETERMINATION OF THE EFFECT OF HORIZONTAL-TAIL SIZE, TAIL LENGTH, AND VERTICAL LOCATION ON LOW-SPEED STATIC LONGITUDINAL STABILITY AND DAMPING IN PITCH OF A MODEL HAVING 45° SWEPTBACK WING AND TAIL SURFACES [1]

By Jacob H. Lichtenstein

SUMMARY

An investigation has been conducted in the Langley stability tunnel to determine the effects of horizontal tails of various sizes and at various tail lengths (when located on the fuselage center line) and also the effects of vertical location of the horizontal tail relative to the wing on the low-speed static longitudinal stability and on the steady-state rotary damping in pitch for a complete-model configuration. The wing and tail surfaces had the quarter-chord lines swept back 45° and had aspect ratios of 4.

The results of the investigation showed that, in agreement with analytical considerations, the contribution of the horizontal tail to static longitudinal stability was related directly to the tail size and length; whereas, its contribution to damping in pitch was related directly to tail size and the square of tail length.

At low angles of attack, addition of the wing decreased the contribution of the horizontal tail to static longitudinal stability by about one-half to one-third depending upon the vertical position of the tail relative to the wing; the contribution of the horizontal tail to the rotary damping in pitch on the other hand was almost unaffected by addition of the wing, regardless of tail area or location.

For configurations with the horizontal tail mounted along the fuselage center line, the static longitudinal stability was greater at angles of attack near the stall than at 0°; the static longitudinal characteristics were impaired, however, by moving the horizontal tail upward. On the other hand, for configurations with the horizontal tail mounted along the fuselage center line, the rotary damping in pitch was less at angles of attack near the stall than at 0°, but the damping in pitch was generally increased by moving the tail upward.

It was further indicated that, at an angle of attack of about 10°, the static longitudinal stability of the wing-fuselage combination changed adversely and that the magnitude of this change was slightly increased by the addition of tail area along the fuselage center line at the shortest tail length but was decreased by addition of area along the fuselage center line at the longest tail length.

INTRODUCTION

Requirements for satisfactory high-speed performance of aircraft have resulted in configurations that differ in many respects from previous designs. As a result of these changes, the designer has little assurance that the low-speed characteristics will be satisfactory for any specific configuration. The low-speed characteristics of wings suitable for high-speed flight have already been investigated quite extensively. The contributions of other component parts of the aircraft, or of the various combinations of component parts for high-speed airplane configurations, however, are not well understood. In order to provide such information, a series of investigations of models having various interchangeable component parts is being conducted in the Langley stability tunnel. In these investigations, the rotary derivatives are being determined by the rolling- and curved-flow techniques (see references 1 and 2) and the static stability characteristics are being determined by conventional wind-tunnel procedure.

The present investigation is concerned with the effects of horizontal tails of various sizes and at various tail lengths (when located on the fuselage center line) and also the effects of vertical location of the horizontal tail with respect to the wing on the low-speed static longitudinal stability and the steady-state rotary damping in pitch for a swept-wing configuration. Some effects of fuselage fineness ratio and of wing-fuselage interference are also considered. The rotary damping in pitch specifies the damping resulting only from curvature of the flight path, such as that obtained during a steady pitching maneuver in which the radius of flight-path curvature is constant. For a pitching oscillation, the rotary damping derivative represents only a part of the total damping since additional contributions may result from unsteady aerodynamic phenomena such as the lag of downwash between the wing and horizontal tail (references 3 and 4).

The model used in the present investigation had 45° sweptback wing and horizontal-tail surfaces with aspect ratios of 4. The model configurations tested for the present investigation are generally the same as those configurations used in the investigations of static lateral stability derivatives reported in references 5 and 6.

SYMBOLS

The data presented herein are in the form of standard NACA coefficients of forces and moments which are referred to the stability system of axes, with the origin at the projection on the plane of symmetry of the quarter-chord

[1] Supersedes NACA TN 2381, "Effect of Horizontal-Tail Location on Low-Speed Static Longitudinal Stability and Damping in Pitch of a Model Having 45° Sweptback Wing and Tail Surfaces" by Jacob H. Lichtenstein, 1951, and NACA TN 2382, "Effect of Horizontal-Tail Size and Tail Length on Low-Speed Static Longitudinal Stability and Damping in Pitch of a Model Having 45° Sweptback Wing and Tail Surfaces" by Jacob H. Lichtenstein, 1951.

point of the mean aerodynamic chord of the wing. The positive directions of the forces, moments, angles, and angular velocities are shown in figure 1. The coefficients and symbols are defined as follows:

C_L lift coefficient $\left(L/\frac{1}{2}\rho V^2 S_W\right)$

C_D drag coefficient $\left(D/\frac{1}{2}\rho V^2 S_W\right)$

C_m pitching-moment coefficient $\left(M/\frac{1}{2}\rho V^2 S_W \bar{c}_W\right)$

C_n yawing-moment coefficient $\left(N/\frac{1}{2}\rho V^2 S_W b_W\right)$

L lift, pounds

D drag, pounds

M pitching moment about $\bar{c}_W/4$, foot-pounds

N yawing moment about Z-axis, foot-pounds

ρ mass density, slugs per cubic foot

V velocity, feet per second

S area, square feet

b span, measured perpendicular to fuselage center line, feet

c chord, measured parallel to axis of symmetry, feet

$\bar{c}$ mean aerodynamic chord, feet $\left(\frac{2}{S}\int_0^{b/2} c^2 dy\right)$

l tail length, distance from $\bar{c}_W/4$ to $\bar{c}_H/4$, measured parallel to axis of symmetry, feet

A aspect ratio (b^2/S)

y spanwise distance from plane of symmetry, feet

λ taper ratio, ratio of tip chord to root chord

α angle of attack, measured in plane of symmetry, degrees

v_F fuselage volume

L_F fuselage length

d_F maximum fuselage diameter

ϵ effective downwash angle, degrees

ψ angle of yaw, degrees

q pitching angular velocity, radians per second

$\frac{qc}{2V}$ pitching-velocity parameter (based on $\bar{c}_W$)

$C_{L_\alpha} = \frac{\partial C_L}{\partial \alpha}$

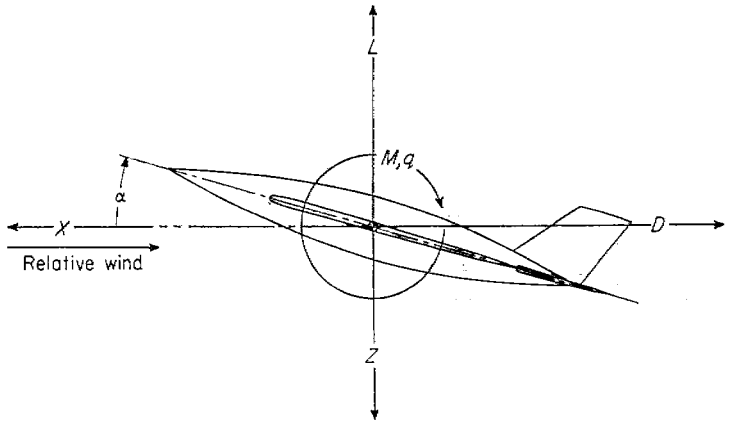

FIGURE 1.—System of axes used. Arrows indicate positive direction of forces, moments, angles, and angular velocities.

$C_{m_\alpha} = \frac{\partial C_m}{\partial \alpha}$

$C_{m_{\dot{\alpha}}} = \frac{-\partial C_m}{\partial\left(\frac{\dot{\alpha}c}{2V}\right)}$, where $\dot{\alpha} = \frac{\partial \alpha}{\partial t}$

$C_{m_q} = \frac{\partial C_m}{\partial\left(\frac{qc}{2V}\right)}$

$C_{n_\psi} = \frac{\partial C_n}{\partial \psi}$

$(\Delta C_{m_q})_H$, $(\Delta C_{m_\alpha})_H$ increment resulting from addition of horizontal tail; for example,

$$(\Delta C_{m_q})_H = (C_{m_q})_{Model\ with\ H} - (C_{m_q})_{Model\ without\ H}$$

$\Delta_1 C_{m_q}$, $\Delta_1 C_{m_\alpha}$ increment resulting from interference effect of wing and fuselage; for example, $\Delta_1 C_{m_q} = (C_{m_q})_{W+F} - (C_{m_q})_W - (C_{m_q})_F$

Subscripts:

W wing

F fuselage

V vertical tail

H horizontal tail

r radian measure

APPARATUS, MODELS, AND TESTS

The general research model used for the present investigation was designed to permit tests of the wing alone, fuselage alone, or the fuselage in combination with any of several tail configurations—with or without the wing. A sketch with some dimensions of the complete model with one particular tail configuration is shown in figure 2. A list of the pertinent geometric characteristics of various component parts is given in table I. All of the parts were constructed of mahogany.

Three fuselages and three horizontal tails were used for the tests in various combinations with and without the wing. For convenience, each component is designated as follows:

W	Wing
F_1, F_2, F_3	Fuselages
V	Vertical tail
H_1, H_2, H_3	Horizontal tails

A complete list of all the configurations investigated is presented in table II.

The three fuselages (fig. 3) were bodies of revolution having circular-arc profiles and fineness ratios of 5 for fuselage 1, 6.67 for fuselage 2, and 10 for fuselage 3. The wing and the three horizontal-tail surfaces all had aspect ratios of 4.0, taper ratios of 0.6, and NACA 65A008 airfoil sections parallel to the plane of symmetry; the quarter-chord lines were swept back 45°. Ordinates for the NACA 65A008 airfoil section are given in table III. The horizontal tails, the incidence of which was kept at 0° for all tests, differed from each other only in area and are designated as H_1, H_2, and H_3 (in order of increasing size) in figure 4 and table I. On each

of the fuselages, each of the three horizontal-tail surfaces was attached along the fuselage center line and at the same longitudinal location. On fuselage 2, however, horizontal tail 2 was tested at three horizontal locations for each of three vertical locations, as illustrated in figure 5. In reference to the horizontal-tail locations, the letters L, C, and U indicate the vertical position as being lower, center, or upper, respectively; the letters F, M, and R indicate the horizontal location as being forward, middle, or rearward, respectively. The lower middle position is the same as that at which the other two horizontal tails were tested.

A drawing of a complete-model configuration with the horizontal tail in the lower position and a photograph of the model with the horizontal tail in the upper position without a wing are presented in figures 6 (a) and 6 (b), respectively, to illustrate the test setup in the tunnel. The model was rigidly mounted on a three-support-strut system with the pivot point 4 inches rearward of the quarter-chord point of the mean aerodynamic chord. Forces and moments were measured by means of a conventional six-component balance system.

The tests were made in the 6- by 6-foot test section of the Langley stability tunnel. The dynamic pressure for the tests was 24.9 pounds per square foot, which corresponds to a Mach number of 0.13 and to a Reynolds number, based upon the wing mean aerodynamic chord, of 0.71×10^6. The angle of attack was varied from about $-6°$ to about 32° for the tests. In addition to the straight-flow tests, the tunnel flow was curved to obtain values of $qc/2V$ of 0.008, 0.017, and 0.022. The method of curving the flow consists in curving the tunnel walls to obtain the proper air-stream curvature and inserting upstream of the test section screens which give the proper velocity gradient across the test section.

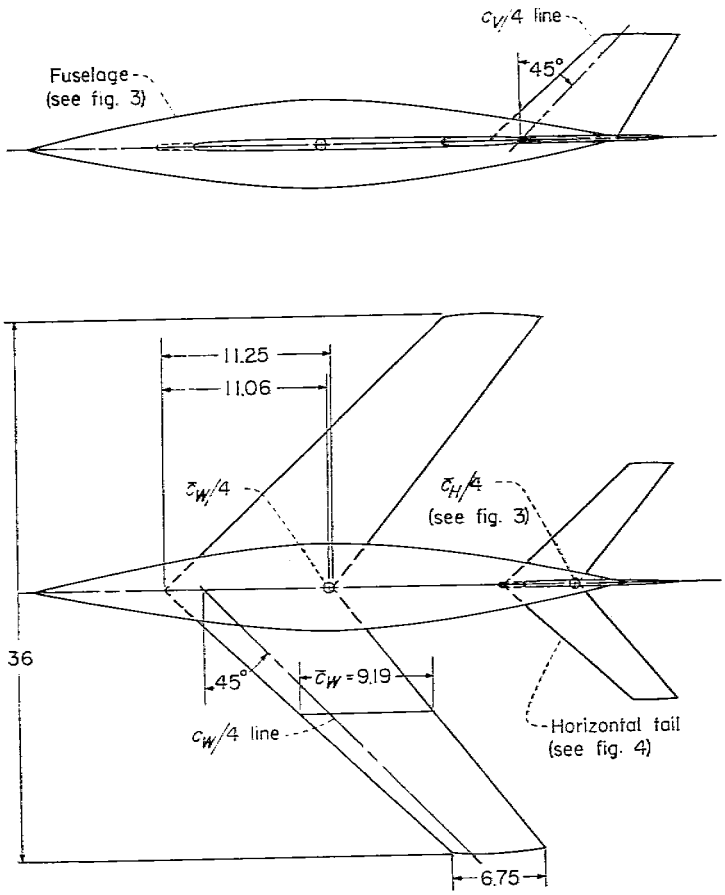

FIGURE 2.—Dimensions of the complete model. All dimensions are in inches.

CORRECTIONS

The angle of attack and drag coefficient have been corrected for the effects of jet boundaries. The moment data have been transferred from the mounting point to the 25-percent point of the wing mean aerodynamic chord. The damping-in-pitch data have been corrected for the effects of the cross-tunnel static-pressure gradient associated with the curved flow. The data have not been corrected for blocking, turbulence, or support-strut interference since, for the parameters with which this report is concerned, these effects are believed to be negligible.

TABLE I

PERTINENT GEOMETRIC CHARACTERISTICS OF THE MODEL

Fuselage:	F_1	F_2	F_3
Length, in.	30	40	60
Fineness ratio	5	6.67	10
Volume, v_F, cu ft	0.267	0.350	0.526
Wing:			
Aspect ratio, A_W			4.0
Taper ratio, λ_W			0.6
Quarter-chord sweep angle, deg			45
Dihedral angle, deg			0
Twist, deg			0
NACA airfoil section			65A008
Area, S_W, sq in.			324
Span, b_W, in.			36
Mean aerodynamic chord, $\bar{c}_W$, in.			9.19
Vertical tail:			
Aspect ratio, A_V			1.0
Taper ratio, λ_V			0.6
Quarter-chord sweep angle, deg			45
NACA airfoil section			65A008
Area, S_V, sq in.			48.6
Span, b_V, in.			6.97
Mean aerodynamic chord, $\bar{c}_V$, in.			7.12
Area ratio, S_V/S_W			0.150

Horizontal tail:	H_1	H_2	H_3
Aspect ratio, A_H	4.0	4.0	4.0
Taper ratio, λ_H	0.6	0.6	0.6
Quarter-chord sweep angle, deg	45	45	45
Dihedral angle, deg	0	0	0
Twist, deg	0	0	0
NACA airfoil section	65A008	65A008	65A008
Area, S_H, sq in.	32.40	64.80	97.20
Span, b_H, in.	11.38	16.10	19.72
Mean aerodynamic chord, $\bar{c}_H$, in.	2.91	4.11	5.04
Area ratio, S_H/S_W	0.10	0.20	0.30

Tail-length ratio $l/\bar{c}_W$:

Fuselage	F_1	F_2			F_3
Position of tail:		Forward	Middle	Rearward	
Upper	----	2.42	2.58	2.75	----
Center	----	2.07	2.24	2.40	----
Lower (fuselage center line)	1.36	1.66	1.82	1.98	2.73

TABLE II

CONFIGURATIONS INVESTIGATED AND INDEX TO THE FIGURES HAVING DATA FOR THESE CONFIGURATIONS

Wing off		Wing on	
Configuration (a)	Figure	Configuration (a)	Figure
		W	7
F_1	8(a)	$W+F_1$	9(a)
		$W+F_1+V+H_1$	9(a), 12
F_1+V+H_2	8(a), 12	$W+F_1+V+H_2$	9(a), 12
		$W+F_1+V+H_3$	9(a), 12
F_2	8(b)	$W+F_2$	9(b)
		$W+F_2+V+H_1$	9(b), 12
		$W+F_2+V+H_{2LF}$	10(a), 13
F_2+V+H_2	8(b), 12, 13	$W+F_2+V+H_{2LM}$	9(b), 10 (a), 12, 13
		$W+F_2+V+H_{2LR}$	10(a), 13
		$W+F_2+V+H_{2CF}$	10(b), 13
		$W+F_2+V+H_{2CM}$	10(b), 13
		$W+F_2+V+H_{2CR}$	10(b), 13
		$W+F_2+V+H_{2UF}$	10(c), 13
		$W+F_2+V+H_{2UM}$	10(c), 13
		$W+F_2+V+H_{2UR}$	10(c), 13
		$W+F_2+V+H_3$	9(b), 12
F_3	8(c)	$W+F_3$	9(c)
		$W+F_3+V+H_1$	9(c), 12
F_3+V+H_2	8(c), 12	$W+F_3+V+H_2$	9(c), 12
		$W+F_3+V+H_3$	9(c), 12

[6]Notation:

W wing
F fuselage
V vertical tail
H horizontal tail

} For details, see figures 2 to 5. Subscript numbers 1, 2, and 3 refer to size, subscript letters L, C, and U refer to vertical position of horizontal tail, and letters F, M, and R refer to horizontal location of horizontal tail. (See fig. 5.)

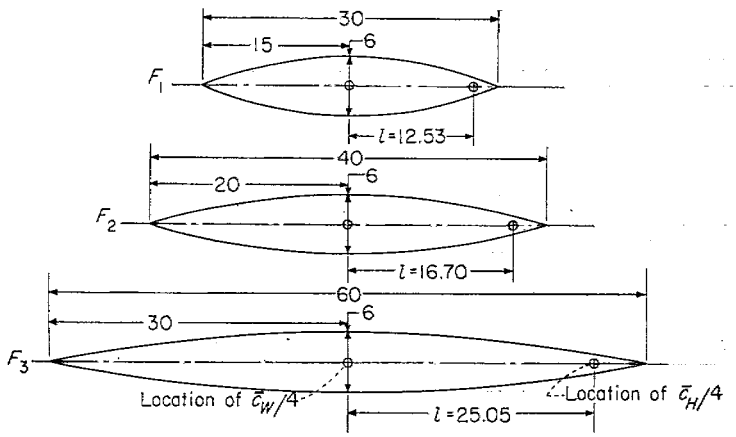

FIGURE 3.—Dimensions of the fuselages tested, and location of the horizontal tail for those tests in which tail area and tail length were of primary concern. All dimensions are in inches.

RESULTS AND DISCUSSION

PRESENTATION OF RESULTS

The basic data obtained in the present investigation are presented in figures 7 to 10. The effect of fuselage fineness ratio on the static longitudinal stability of the fuselage is summarized in figure 11. The effects of tail size and tail length and the effects of tail location on the static longitudinal stability and damping in pitch contributed by the horizontal tail are summarized in figures 12 and 13, respectively.

TABLE III

ORDINATES FOR NACA 65A008 AIRFOIL

[Stations and ordinates in percent airfoil chord]

Station	Ordinate	Station	Ordinate
0	0	40	4.00
.50	.62	45	3.99
.75	.75	50	3.90
1.25	.95	55	3.71
2.50	1.30	60	3.46
5.00	1.75	65	3.14
7.50	2.12	70	2.76
10	2.43	75	2.35
15	2.93	80	1.90
20	3.30	85	1.43
25	3.59	90	.96
30	3.79	95	.49
35	3.93	100	.02

L. E. radius: 0.408

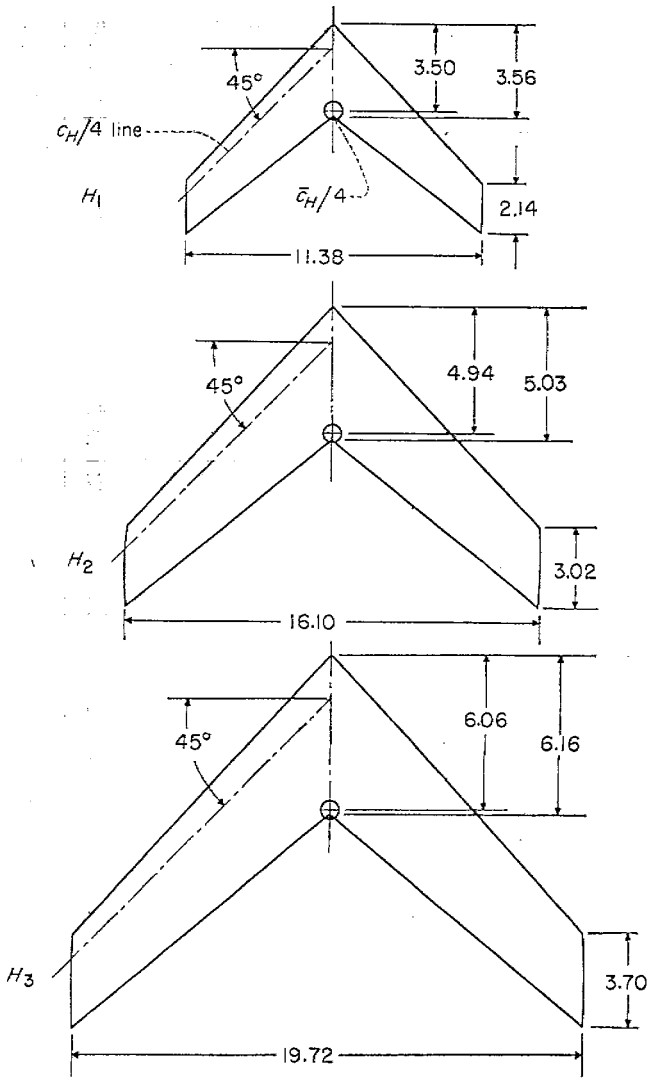

FIGURE 4.—Dimensions of the horizontal tails tested. All dimensions are in inches.

The effect of wing-fuselage interference on both the static longitudinal stability and damping in pitch is shown in figure 14.

An index to the data for the configurations investigated is given in table II.

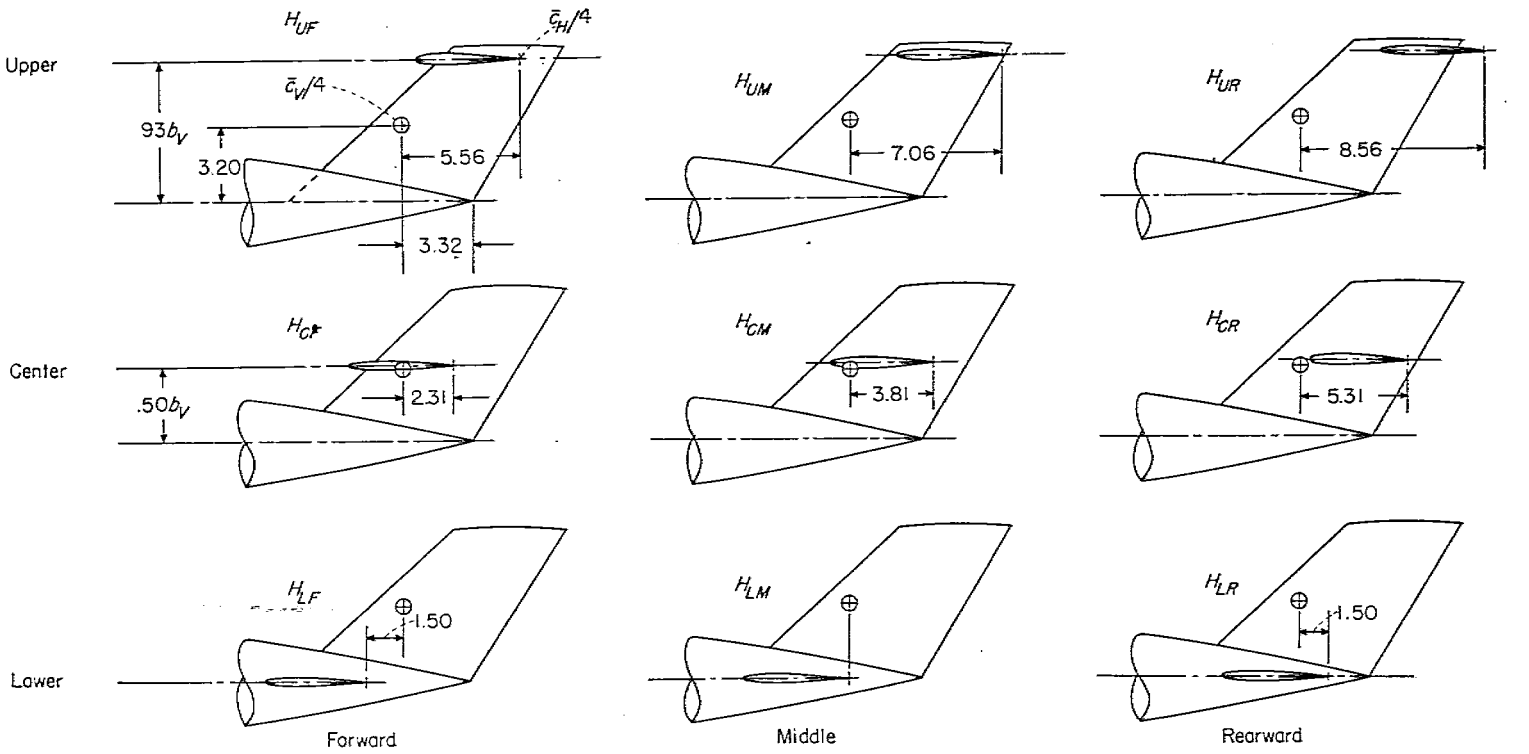

FIGURE 5.—Location of root chord of horizontal tail for the configurations in which vertical location of the horizontal tail was of primary concern. All dimensions are in inches.

STATIC LONGITUDINAL STABILITY

The static longitudinal stability characteristics for some basic configurations are presented in figure 7. Inasmuch as these results are very similar to those presented in reference 5 and analyses of these results are adequately covered in this reference, they are not discussed in this report.

Data are not presented for the lift and drag of the model with each fuselage and horizontal-tail arrangement investigated since the results showed that the lift and drag were only slightly affected by the changes in fuselage and tail. The lift and drag data presented in figure 7 for the configuration $W+F_2+V+H_{2LM}$ are representative of the lift and drag results for all the complete-model configurations.

The pitching-moment characteristics of the three isolated fuselages are presented as a function of angle of attack in figure 8 and are summarized for $\alpha=0°$ in figure 11. In order that the results obtained may be applied conveniently to arbitrary airplane configurations, coefficients in terms of fuselage dimensions rather than wing dimensions are needed. This manner of expressing the coefficient is accomplished by plotting the quantity $(C_{m_\alpha})_F \frac{S_W \bar{c}_W}{v_F}$ against fuselage fineness ratio $\frac{L_F}{d_F}$. The quantity plotted, therefore, is effectively the pitching-moment coefficient based upon fuselage volume v_F. For a body of revolution at an angle of attack of 0°, the value $(C_{m_\alpha})_F \frac{S_W \bar{c}_W}{v_F}$ is the same as $(C_{n_\psi})_F \frac{S_W b_W}{v_F}$; therefore, the results from the present investigation can be compared with the directional-stability data presented in figure 16 of reference 6. The data from the present tests show the same trend as the data of reference 6 but are somewhat larger in magnitude. The difference probably results from the different methods for supporting the models in the tunnel. Comparison of the test data with calculations made by the classical theory of reference 7 shows that, although the variation with fineness ratio is generally similar, the magnitude of the test values is only about four-fifths of that predicted by theory.

The data in figure 8 show that the fuselage-horizontal-tail combination was statically stable as would be expected and that the stability was greater for the large fuselages. In each case, the value of C_{m_α} was constant up to angles of attack of about 16°, at which point the lift-curve slope of the horizontal tail begins to decrease appreciably.

Addition of any of the fuselages to the wing had little effect on C_{m_α}, as can be seen by comparison of figures 7 and 9. The fact that the wing-fuselage combination had approximately the same longitudinal stability as the wing alone may be attributed to the loss in load over the wing near the wing-fuselage juncture and to the alteration in fuselage loading effected by upwash in front of the wing.

For the complete-model configurations with the horizontal tail mounted on the fuselage center line, a destabilizing change in the slope of C_{m_α} generally occurs at an angle of attack of about 10°. For the shortest tail length (fuselage F_1, fig. 9(a)), the magnitude of the change in slope apparently was increased slightly as the horizontal-tail area was increased. For the longest tail length (fuselage F_3, fig. 9(c)), an increase in tail area caused a decrease in this destabilizing change in slope; in fact, this change apparently was eliminated by the addition of the two largest tails (H_2 or H_3). This

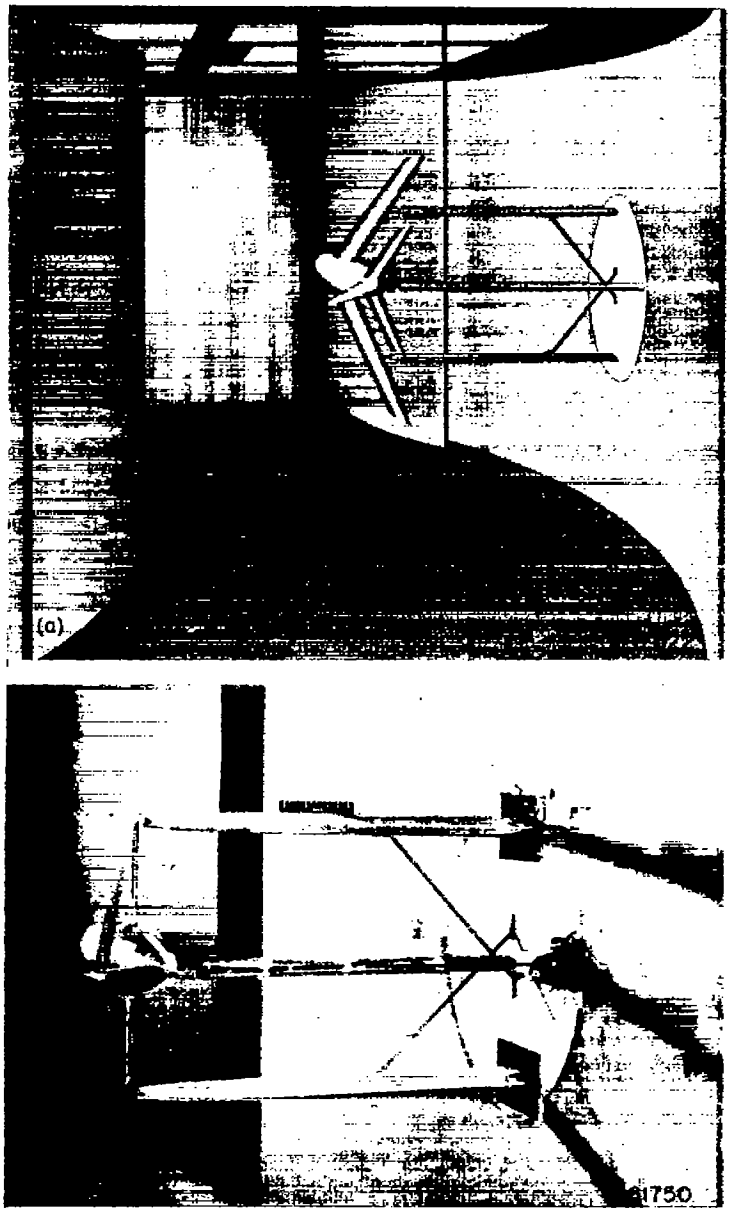

(a) Complete-model configuration with the horizontal tail in the low position.
(b) Fuselage with the horizontal tail in the upper rear position.

FIGURE 6.—Illustration of the model setup in the Langley stability tunnel for testing in curved flow.

effect of tail length on the manner in which addition of tail area affects the longitudinal stability appears to be primarily a matter of geometry in that, for a given location of the tail relative to the fuselage center line, the tail length determines the vertical location of the tail relative to the wing wake at a particular angle of attack. The destabilizing tendency for the wing-fuselage combination at an angle of attack of about 10° results from tip stalling of the wing, and, as a result of this stalling, the wing trailing vortices move inward with an associated increase in downwash in the wake at the plane of symmetry. For the short tail length, the tail is sufficiently close to the wake at an angle of attack of 10° to experience destabilizing effects. For the longest tail length, however, the tail has emerged sufficiently from the wake to avoid the effect of the increased downwash. It can be seen, therefore, that increasing the tail area for the short tail length would be adverse, whereas for the long tail length it would be beneficial.

The data of figure 10 show that relatively small rearward movement of the horizontal tail in any of the vertical positions (low, center, or upper) generally resulted in slightly more negative values of C_{m_α} (increased stability) as would be expected because of the increase in tail length. Raising the horizontal tail also made C_{m_α} more negative in the low angle-of-attack range; however, it made C_{m_α} more positive (decreased stability) in the angle-of-attack range between 10° and 20°. These results are in general similar to results of previous investigations of like nature at both low and high Reynolds numbers (reference 8 and data from the Langley 19-foot pressure tunnel). The increase in stability, at low angles of attack, as the horizontal tail is moved upward was greater than would be expected to result from the increase in tail length which accompanied the upward movement of the tail. Part of this increase in stability, therefore, appears to result from the fact that, in the higher positions, the horizontal tail was above the region of strongest downwash, as is shown in a subsequent section discussing the contribution of the horizontal tail. As the angle of attack increases, however, the horizontal tails mounted in the high positions move into the strong downwash field; whereas, the tails in the low position emerge from the downwash field. This can be seen quite easily by comparing the pitching-moment curves between 12° and 20° for the configurations $W+F_3+V+H_2$ (fig. 9(c)) and $W+F_3+V+H_{2UR}$ (fig. 10(c)) which have about the same tail-length ratio. The data show that the low tail position is almost completely free of the downwash effects, whereas the upper position is very strongly affected by the downwash.

The data in figures 9 and 10 show that the static longitudinal stability was generally greater at angles of attack near the stall than for any other part of the angle-of-attack range.

From the standpoint of static longitudinal stability, the low horizontal-tail positions appear to be more advantageous than the high tail positions because the change in stability is smallest over the angle-of-attack range, and, for configurations with the tail in the low position, the farther rearward the horizontal tail is located the less likely it is to be influenced by the wing downwash.

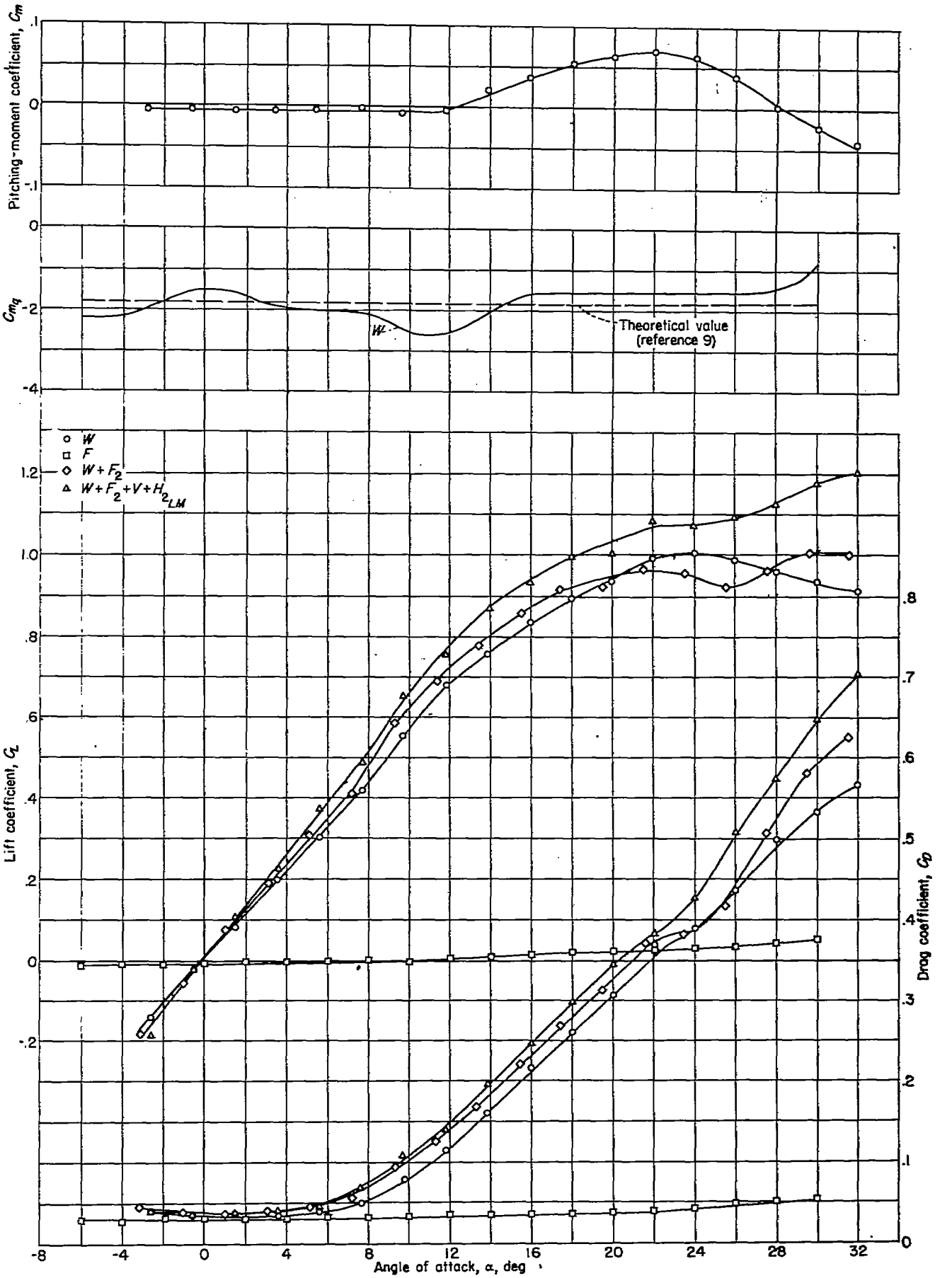

FIGURE 7.—Aerodynamic characteristics in straight flow of some basic configurations, and damping in pitch for the wing alone.

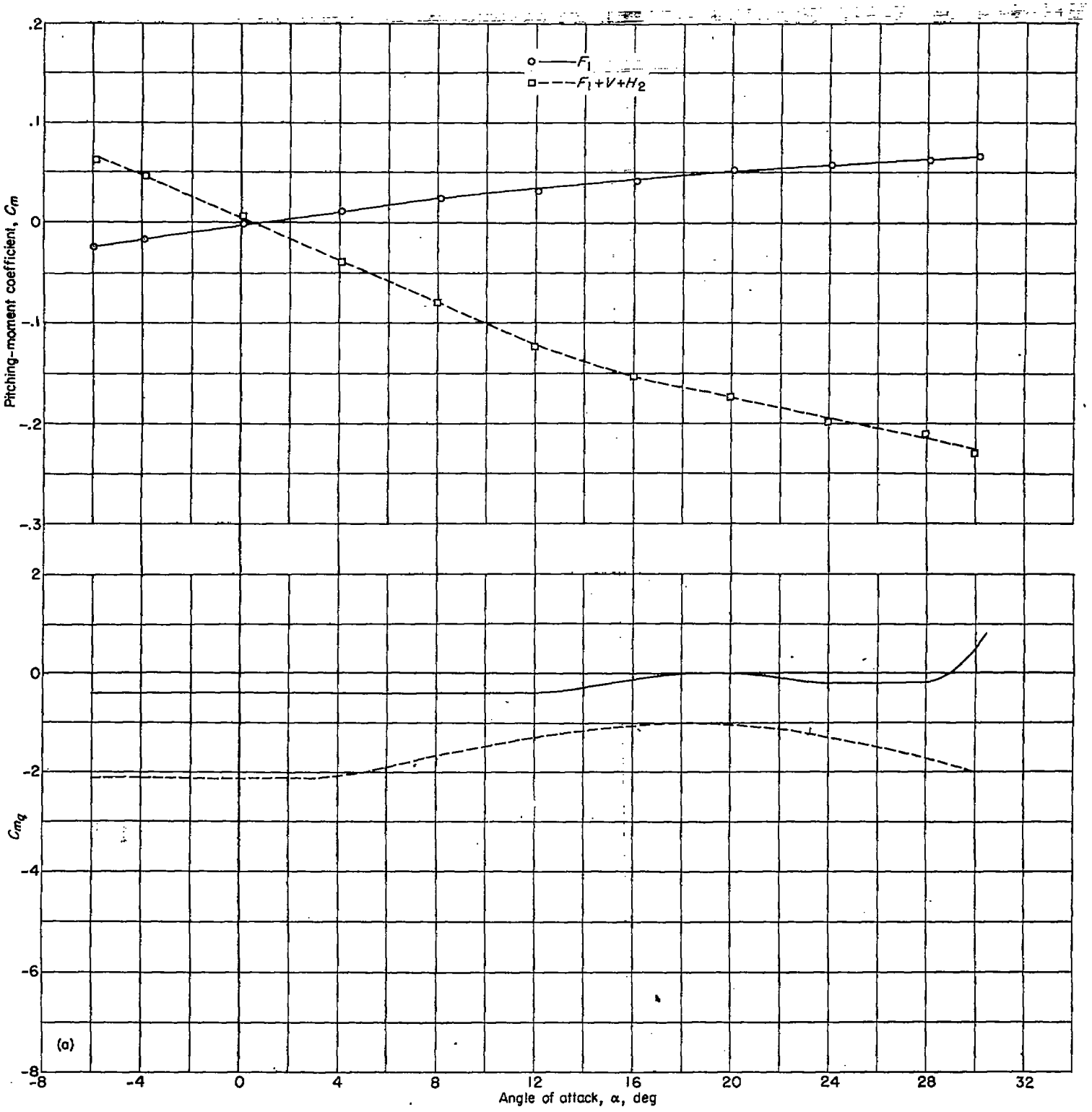

(a) Short fuselage F_1.

FIGURE 8.—Variation of static pitching-moment coefficient and damping-in-pitch coefficient with angle of attack for wing-off configurations.

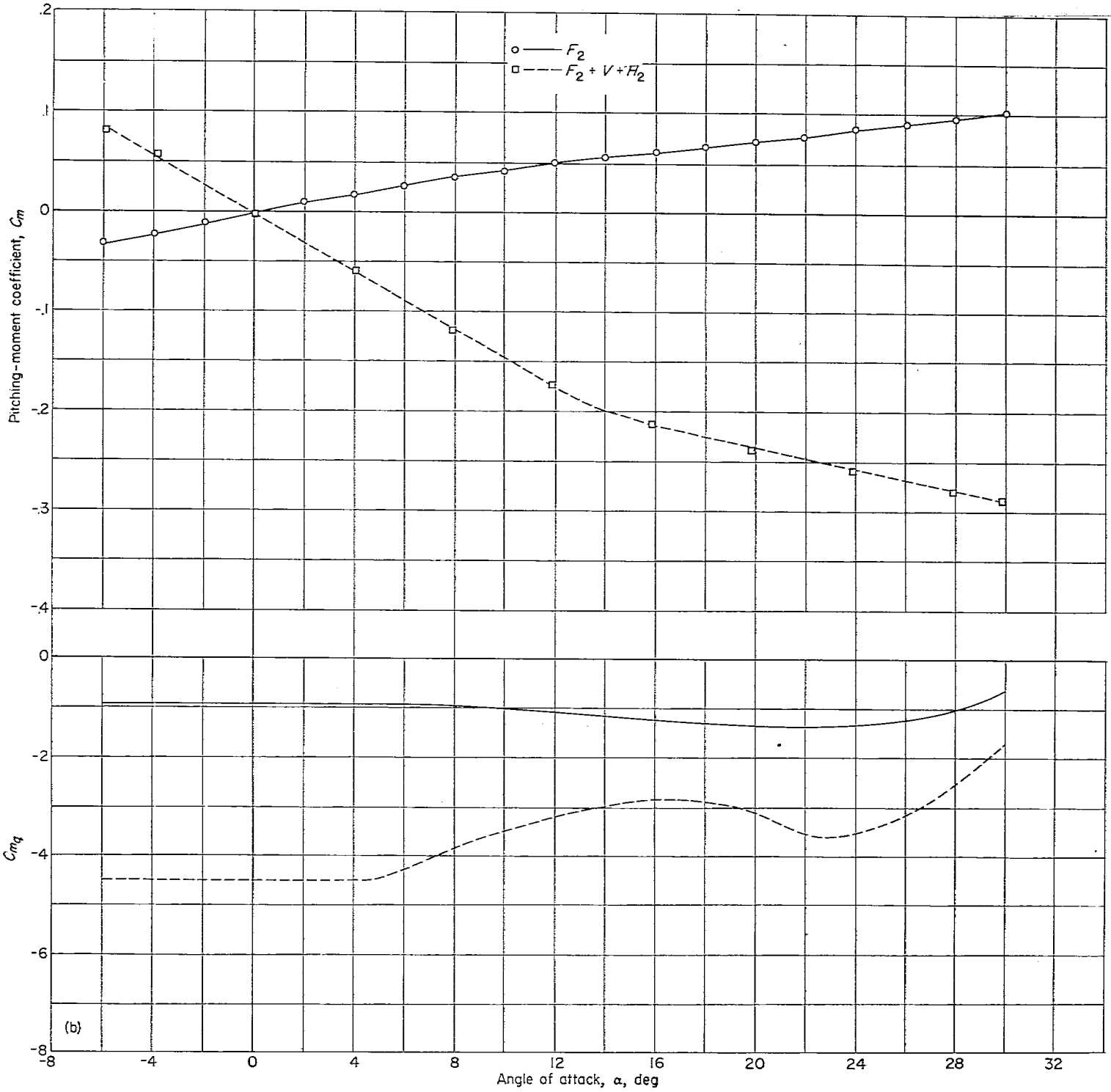

(b) Medium fuselage F_2.

FIGURE 8.—Continued.

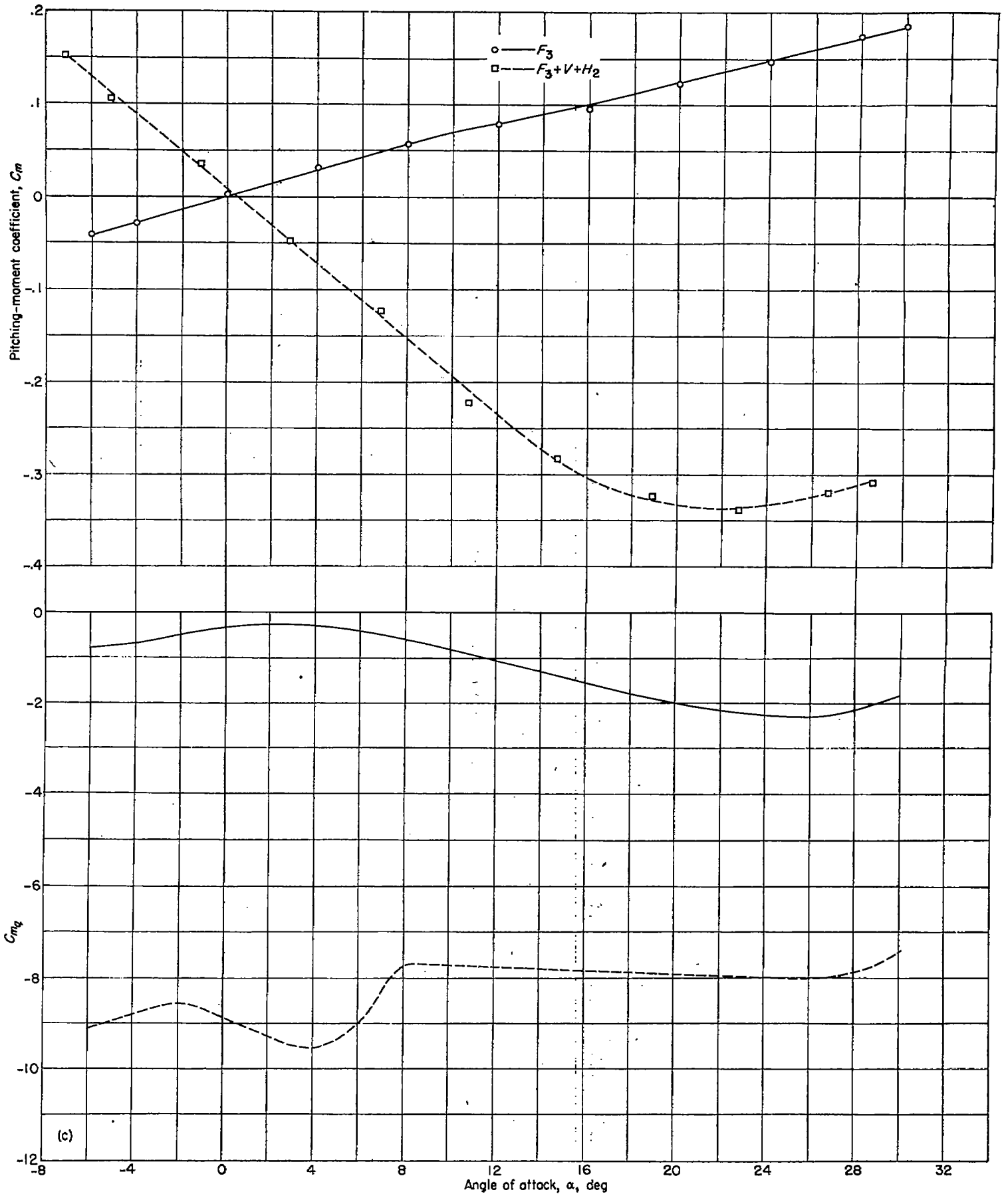

(c) Long fuselage F_3.

FIGURE 8.—Concluded.

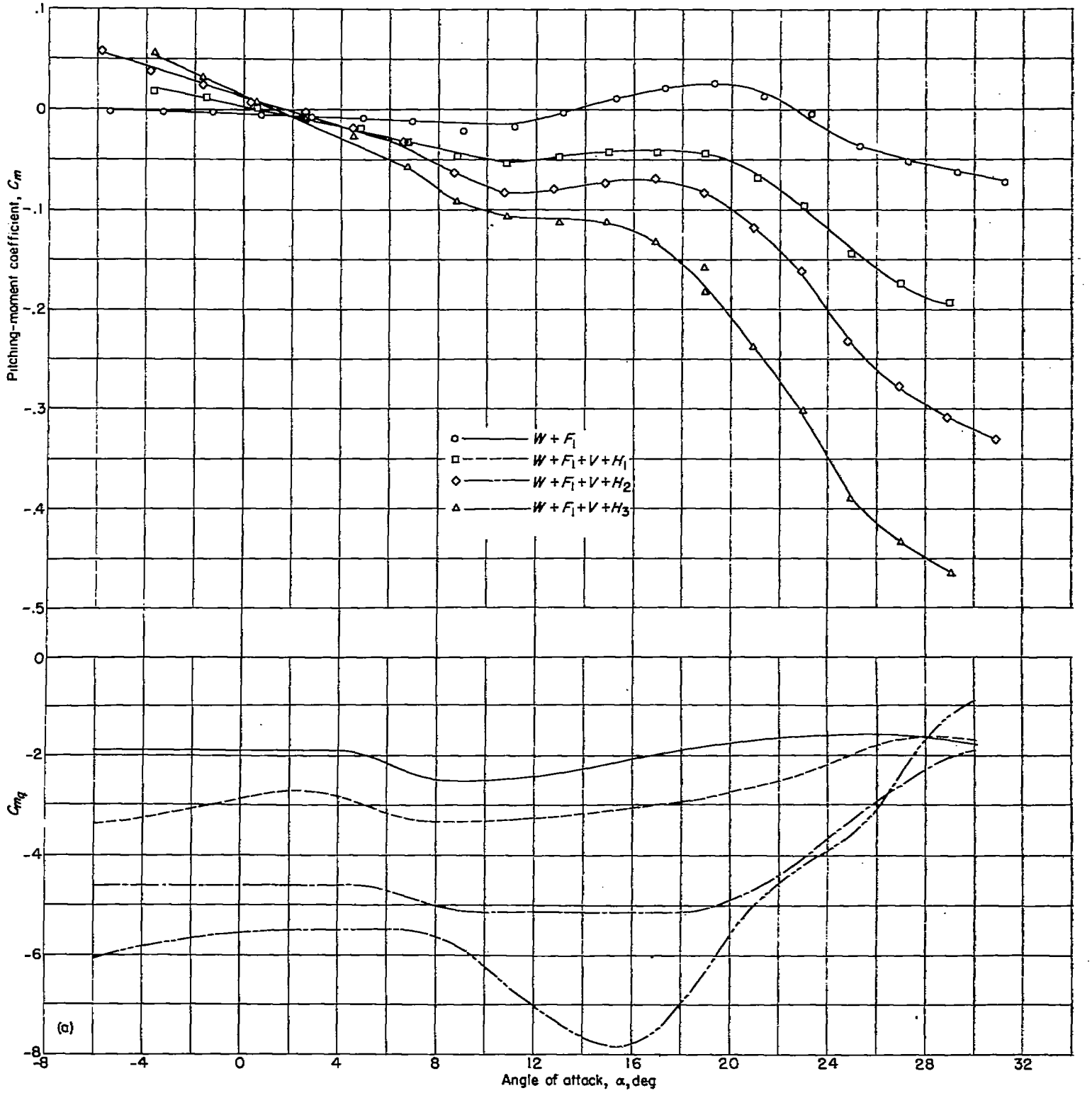

(a) Short fuselage F_1.

FIGURE 9.—Variation of static pitching-moment coefficient and damping-in-pitch coefficient with angle of attack for complete-model configurations in which mainly the horizontal tail area and tail length were varied.

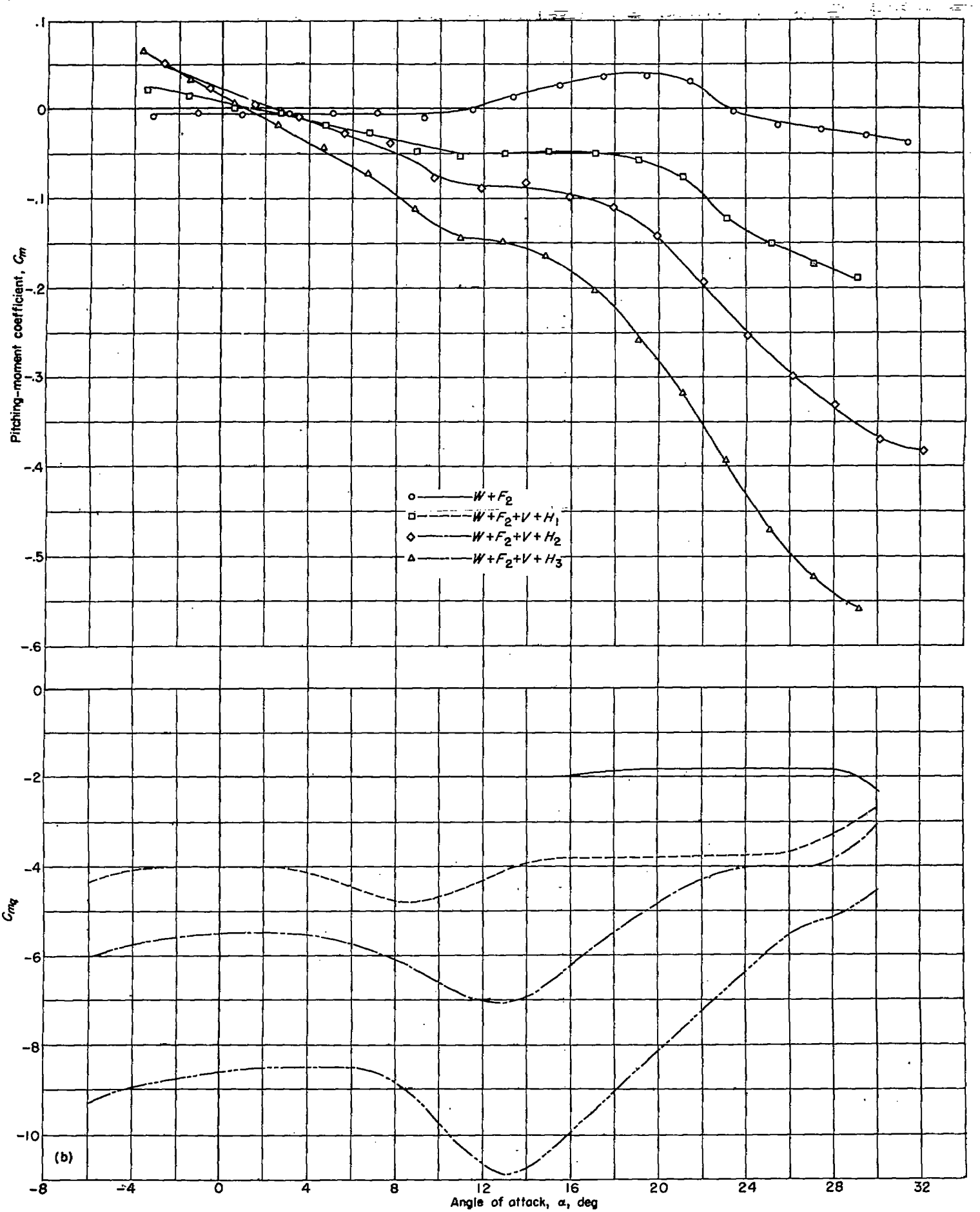

(b) Medium fuselage F_2.

FIGURE 9.—Continued.

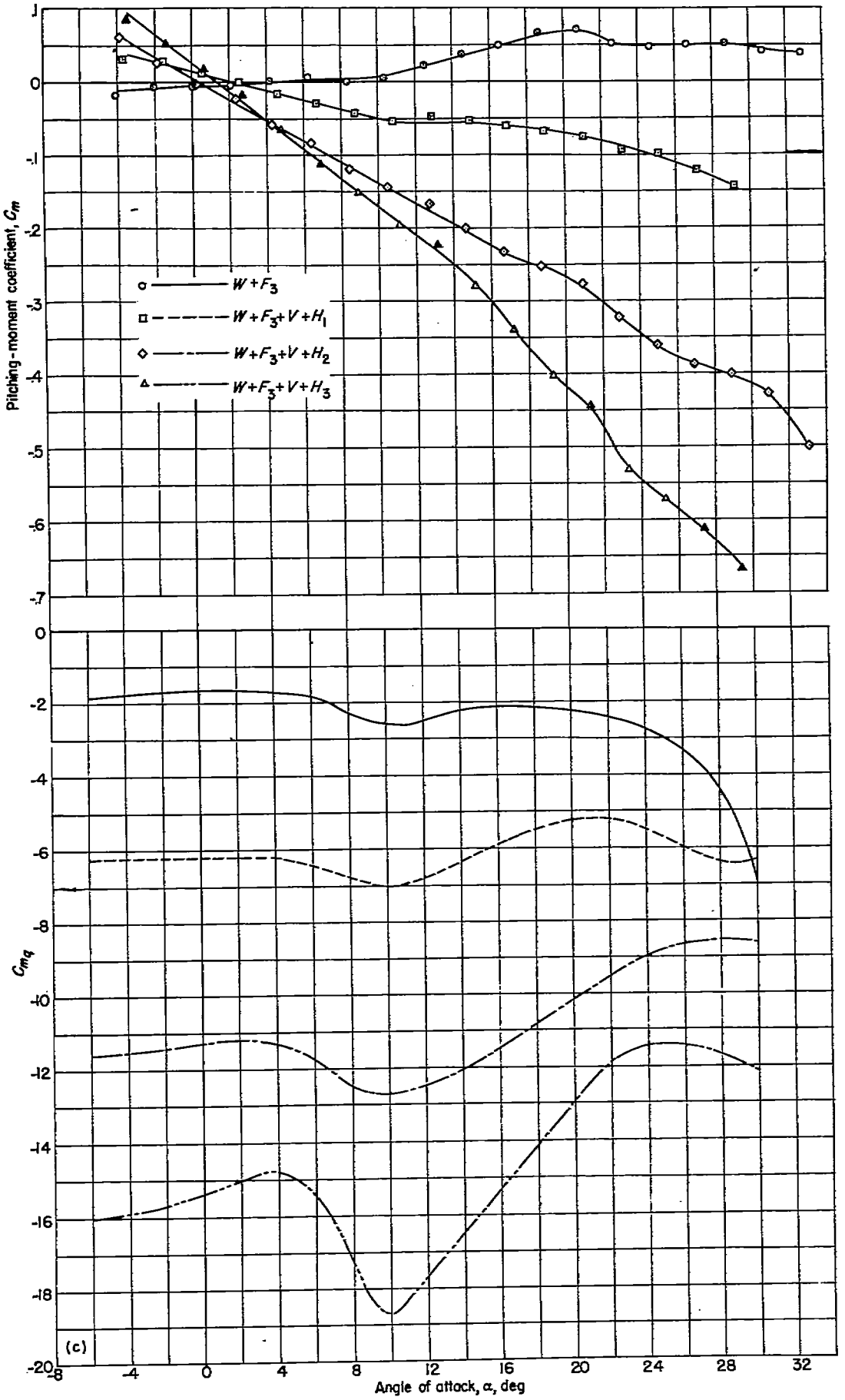

(c) Long fuselage F_3.

FIGURE 9.—Concluded.

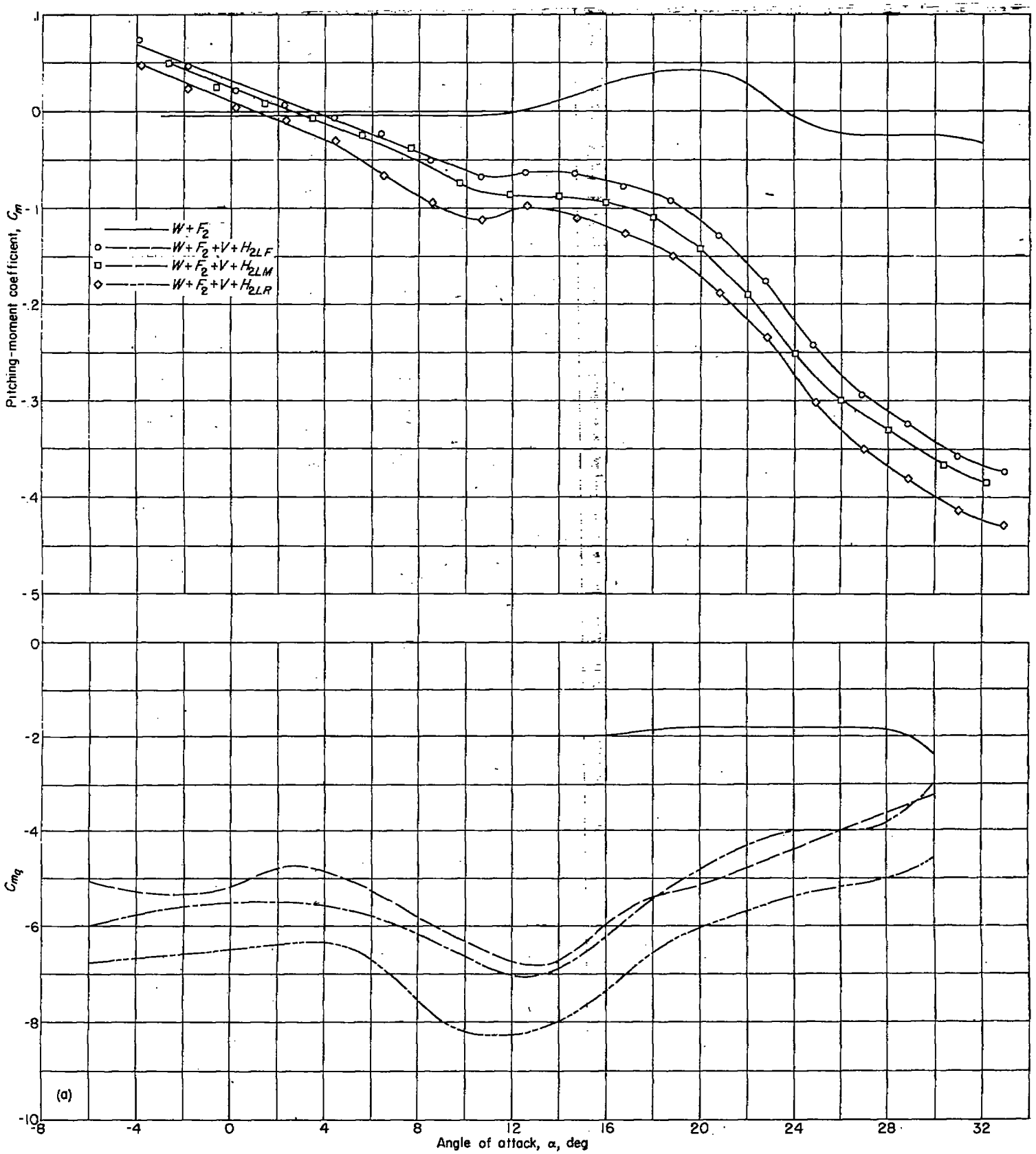

(a) Horizontal tail in the low position.

FIGURE 10.—Variation of static pitching-moment coefficient and damping-in-pitch coefficient with angle of attack for complete-model configurations in which mainly the vertical location of the horizontal tail was varied.

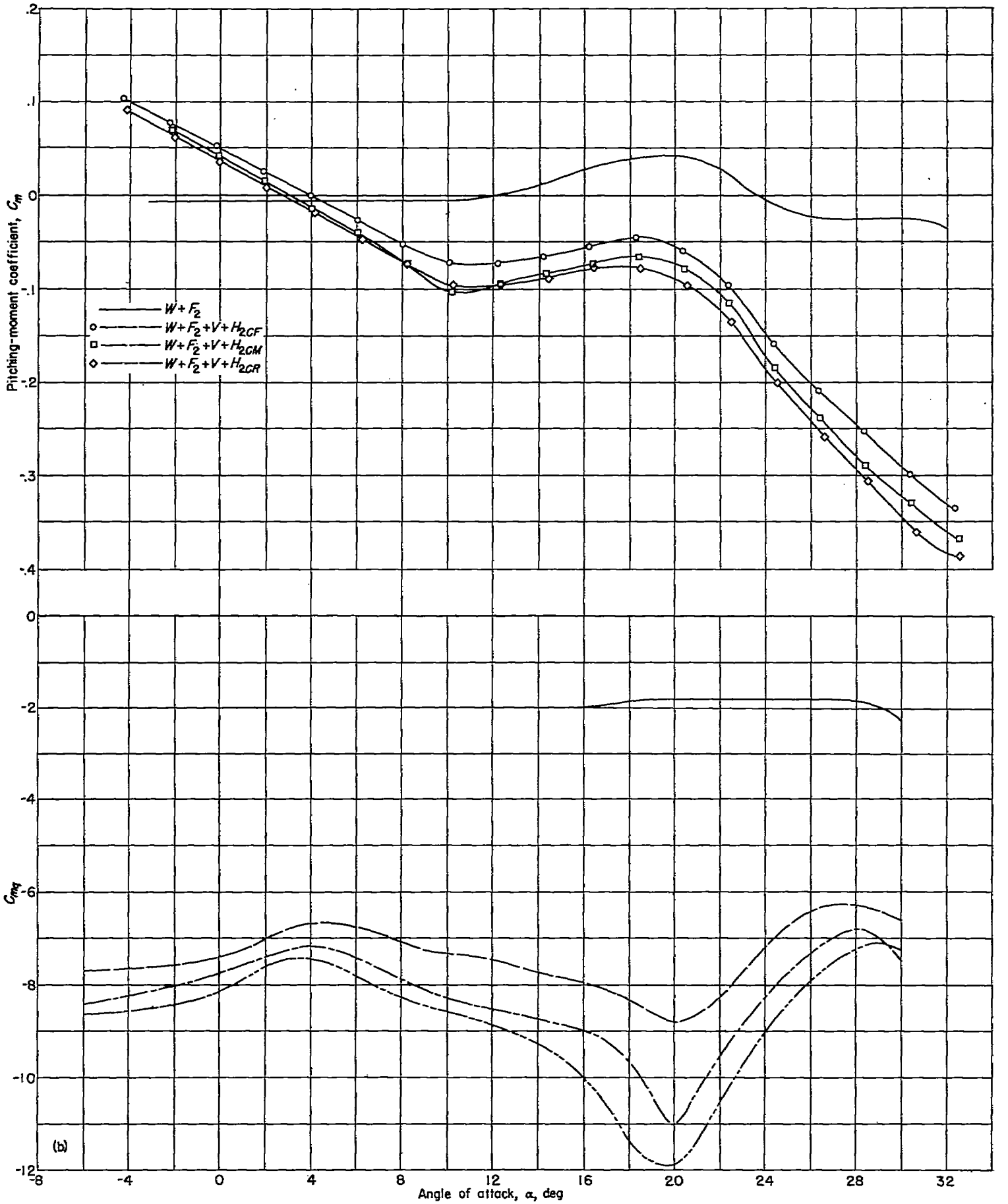

(b) Horizontal tail in the center position

FIGURE 10.—Continued

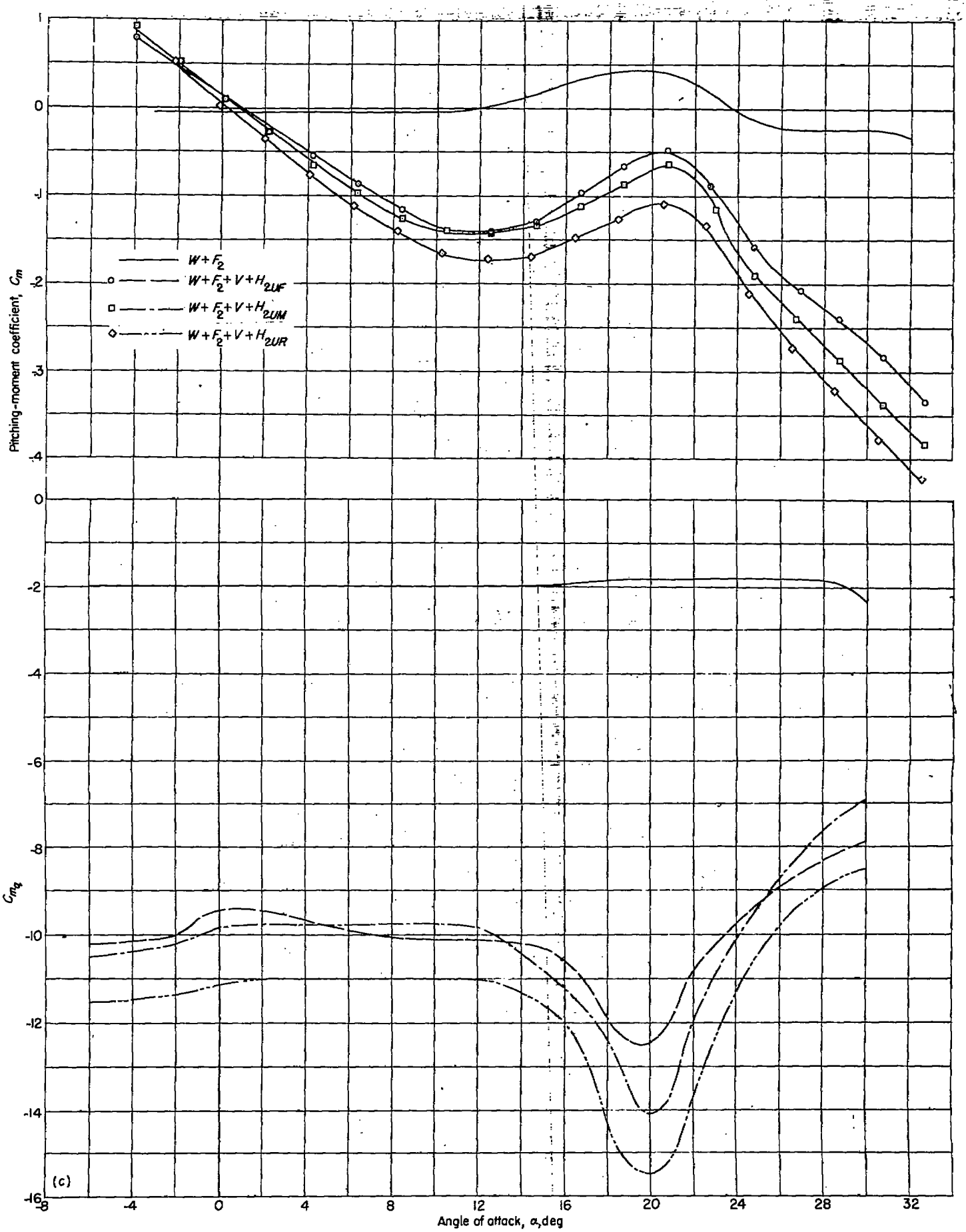

(c) Horizontal tail in the upper position.

FIGURE 10.—Concluded.

DAMPING IN PITCH

The steady-state rotary damping-in-pitch results are presented in figure 7 for the wing alone, in figure 8 for the wing-off configurations, and in figures 9 and 10 for the various complete-model configurations. The value of damping in pitch $-C_{m_q}$ for the wing alone is generally in good agreement with the theoretical value computed by the method presented in reference 9, and the variation with angle of attack is not considered significant. Addition of a fuselage to the wing did not appreciably affect the value of C_{m_q} for angles of attack up to the stall (compare figs. 7 and 9). This effect was similar to that found for the static longitudinal stability of the model for which the value of C_{m_α} for the wing-fuselage combination is about equal to C_{m_α} of the wing alone, even though the isolated fuselage has a rather large positive value of C_{m_α}.

The damping-in-pitch results presented in figure 8 for the isolated fuselages are considered to be of qualitative value only since the accuracy of the measurements is not considered sufficient to yield results of a reasonable percentage accuracy for values as low as those given by the fuselages. The indications are, however, that the fuselages produced damping of the same sign as that normally expected for a horizontal tail and that the variation of the fuselage damping with angle of attack was not particularly significant.

For the wing-off configurations, the damping in pitch generally decreases as the angle of attack increases (fig. 8). With the wing on, however, the damping in pitch reaches a maximum value at some moderate angle of attack and then decreases with further increase in angle of attack. For configurations with the horizontal tail mounted on the fuselage center line (low position), the angle of attack at which maximum damping occurs generally decreases with increasing fuselage length; this trend can best be seen by comparing the curves for the large tail on the various fuselages (fig. 9). Since most of the damping is due to the horizontal tail, any changes in the damping with angle of attack which are caused by the tail are likely to become greater with increasing tail size. It should be noted that, for these configurations, the damping near the stall (approximately 24°) had decreased, in general, to some value considerably less than that at zero lift. For the configurations with the horizontal tail mounted in the center or upper positions, the maximum damping occurred at higher angles of attack (approximately 20°). (See figs. 10 (b) and 10 (c).) The maximum damping would normally be expected to occur at the angle of attack at which the static stability is a maximum (C_{m_α} has its maximum negative value). Comparison of C_m and C_{m_q} curves shows, however, that the opposite occurs (maximum damping occurs approximately where the static stability is a minimum). This apparent incongruity results from the interaction of two opposing effects. The decreased static longitudinal stability (downwash effect) occurs when the horizontal tail approaches the wing wake, and the downwash effect becomes greatest when the tail is passing through the wake (approximately 12° angle of attack for the low tails on F_2 and 20° for the higher tails). There is, however, a favorable variation of downwash with $qc/2V$ because stream curvature displaces the wake upward with respect to the horizontal tail. This favorable effect is greatest when the horizontal tail is immersed in the wake at zero flight-path curvature.

Although the basic data do not show the effect of the vertical position of the horizontal tail clearly, because changes in tail position were accompanied by changes in tail length, the higher horizontal-tail positions appear somewhat more advantageous than the low positions with regard to damping in pitch, inasmuch as the variation with angle of attack was generally smaller and high damping was maintained to nearly maximum lift.

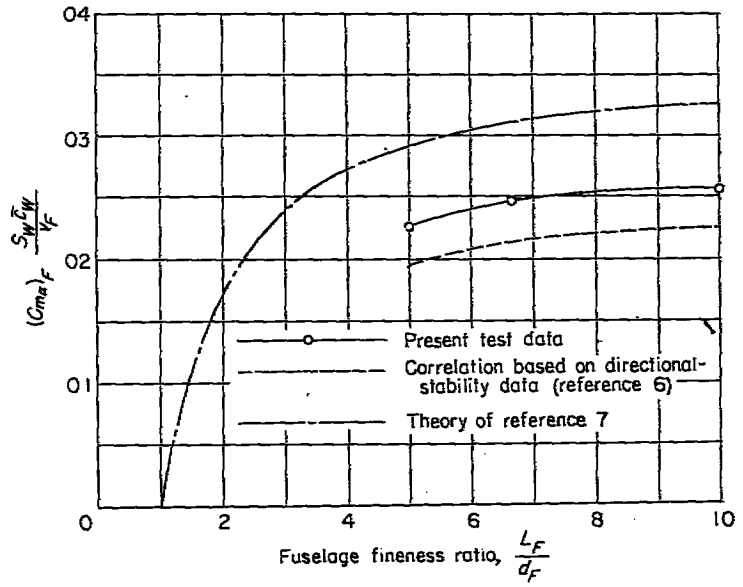

FIGURE 11.—Comparison of the effect of fuselage fineness ratio on the static stability of the fuselage as determined from longitudinal- and directional-stability measurements and from theory. $\alpha=0°$.

CONTRIBUTIONS OF THE HORIZONTAL TAIL

In general, the contributions of a horizontal tail to both static longitudinal stability and damping in pitch are affected by the downwash from the wing and by the local dynamic pressure in the vicinity of the tail. In the absence of a slipstream and of any important flow separation from the wing, the local dynamic pressure is essentially the same as the free-stream dynamic pressure and the downwash remains as the only factor to be considered. For the present model at low angles of attack, therefore, the tail contribution to static longitudinal stability and to the rotary damping in pitch can be expressed by equations developed by conventional methods of analysis. The tail contribution to static longitudinal stability is given by the following simple relation:

$$(\Delta C_{m_\alpha})_H = -(C_{L_\alpha})_H \left(1-\frac{\partial \epsilon}{\partial \alpha}\right)\frac{S_H}{S_W}\frac{l}{\bar{c}_W} \qquad (1)$$

An analogous expression can be derived for the tail contribution to the rotary damping in pitch. The pitching moment due to the tail can be written as

$$(\Delta C_m)_H = -(\Delta\alpha - \epsilon)(C_{L_\alpha})_H \frac{S_H}{S_W}\frac{l}{\bar{c}_W} \qquad (2)$$

where $\Delta\alpha$ is the change in angle of attack at the tail due to flight-path curvature and is given by

$$\Delta\alpha = 57.3 \frac{l}{\bar{c}_W/2} \frac{qc}{2V}$$

The angle ϵ (measured in degrees) is, in this case, the downwash from the wing or other parts of the airplane and results only from flight-path curvature; that is,

$$\epsilon = 57.3 \frac{qc}{2V} \frac{\partial \epsilon_r}{\partial \frac{qc}{2V}}$$

where ϵ_r, the downwash angle in radian measure, is introduced in order to provide consistent dimensions for both numerator and denominator of the ratio $\frac{\partial \epsilon_r}{\partial \frac{qc}{2V}}$. Substitution in equation (2) of the expressions given for $\Delta\alpha$ and ϵ gives the tail contribution to damping in pitch as

$$(\Delta C_{m_q})_H = -114.6\,(C_{L_\alpha})_H \left(1 - \frac{\partial \epsilon_r}{\partial \frac{ql}{V}}\right) \frac{S_H}{S_W} \left(\frac{l}{\bar{c}_W}\right)^2 \qquad (3)$$

Equations (1) and (3) indicate that the tail contributions to static longitudinal stability and to damping in pitch are proportional to the geometric quantities $\frac{S_H}{S_W}\frac{l}{\bar{c}_W}$ and $\frac{S_H}{S_W}\left(\frac{l}{\bar{c}_W}\right)^2$, respectively. For the portion of the tests in which the effects of horizontal-tail size and tail length were of primary concern, the horizontal tail was always mounted in the low position (along the fuselage center line), and the experimental data have been plotted against $\frac{S_H}{S_W}\frac{l}{\bar{c}_W}$ and $\frac{S_H}{S_W}\left(\frac{l}{\bar{c}_W}\right)^2$ in figure 12 for angle of attack equal to zero. For the portion of the

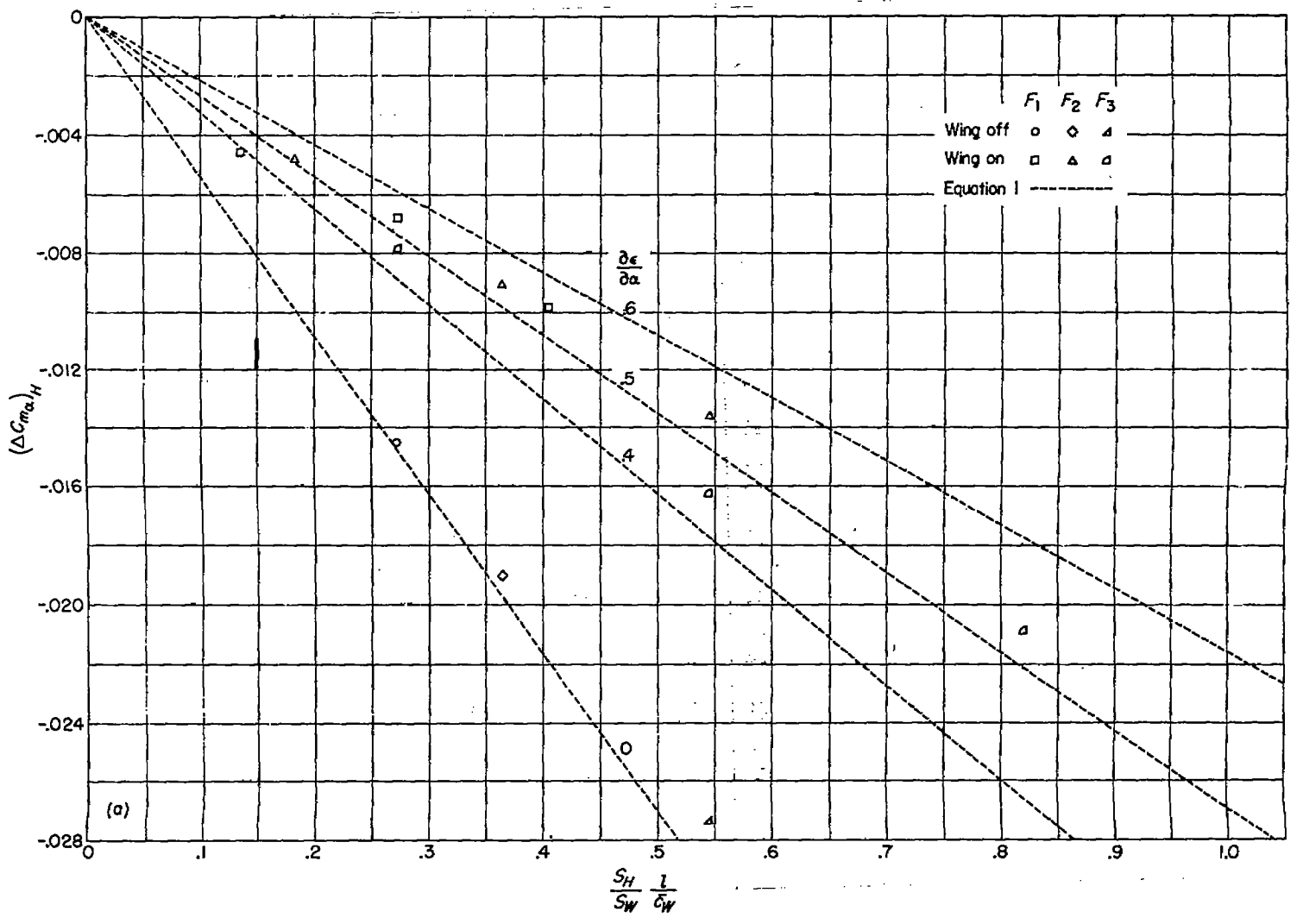

(a) Variation of $(\Delta C_{m_\alpha})_H$ with $\frac{S_H}{S_W}\frac{l}{\bar{c}_W}$.

FIGURE 12.—Variation of the increment in static longitudinal stability and damping in pitch due to the horizontal tail with geometric parameters. Horizontal tail mounted along the fuselage center line. Like symbols indicate horizontal tails of different sizes on the same fuselage. Lift-curve slope of the horizontal tail was assumed to be 0.54. $\alpha = 0°$.

tests in which the effects of tail height were of primary concern, S_H/S_W was maintained constant at 0.2 and, therefore, $l/\bar{c}_W$ and $(l/\bar{c}_W)^2$ were the only geometric variables that entered the equations. The experimental data for this portion of the tests have, accordingly, been plotted against these quantities in figure 13 for angle of attack equal to zero. The dashed curves in figures 12 and 13 were calculated by means of equations (1) and (3) for the values of the downwash parameters $\frac{\partial \epsilon}{\partial \alpha}$ and $\frac{\partial \epsilon_r}{\partial \frac{ql}{V}}$ indicated in the figures.

In the calculations, the tail lift-curve slope $(C_{L_\alpha})_H$ was assumed to have the same value (0.054) as that of the wing alone (fig. 7), since the wing and tail have the same plan form and section. The fact that the curves for the conditions

$$\frac{\partial \epsilon}{\partial \alpha}=\frac{\partial \epsilon_r}{\partial \frac{ql}{V}}=0$$

do not pass through the experimental points obtained with the wing removed shows that the fueselage probably had some influence on the tail effectiveness.

With the wing on and the horizontal tails mounted in the lower position, the data presented in figure 12 (a) indicate that, for the range of configurations considered in this investigation, the value of $\frac{\partial \epsilon}{\partial \alpha}$ is about 0.52. This value is only slightly affected by changes in tail size and length. The data also show that, as indicated by equation (1), the contribution of the horizontal tail to static longitudinal stability varies linearly with tail area and tail length. The data presented in figure 13 (a) indicate that raising the horizontal tail moves it away from the region of strongest downwash since the value of $\frac{\partial \epsilon}{\partial \alpha}$ decreased from 0.52 to about 0.35 as the horizontal tail was moved from the lower to the upper positions.

For wing-on configurations, the data presented in figures 12 (b) and 13 (b) indicate that the value of the downwash

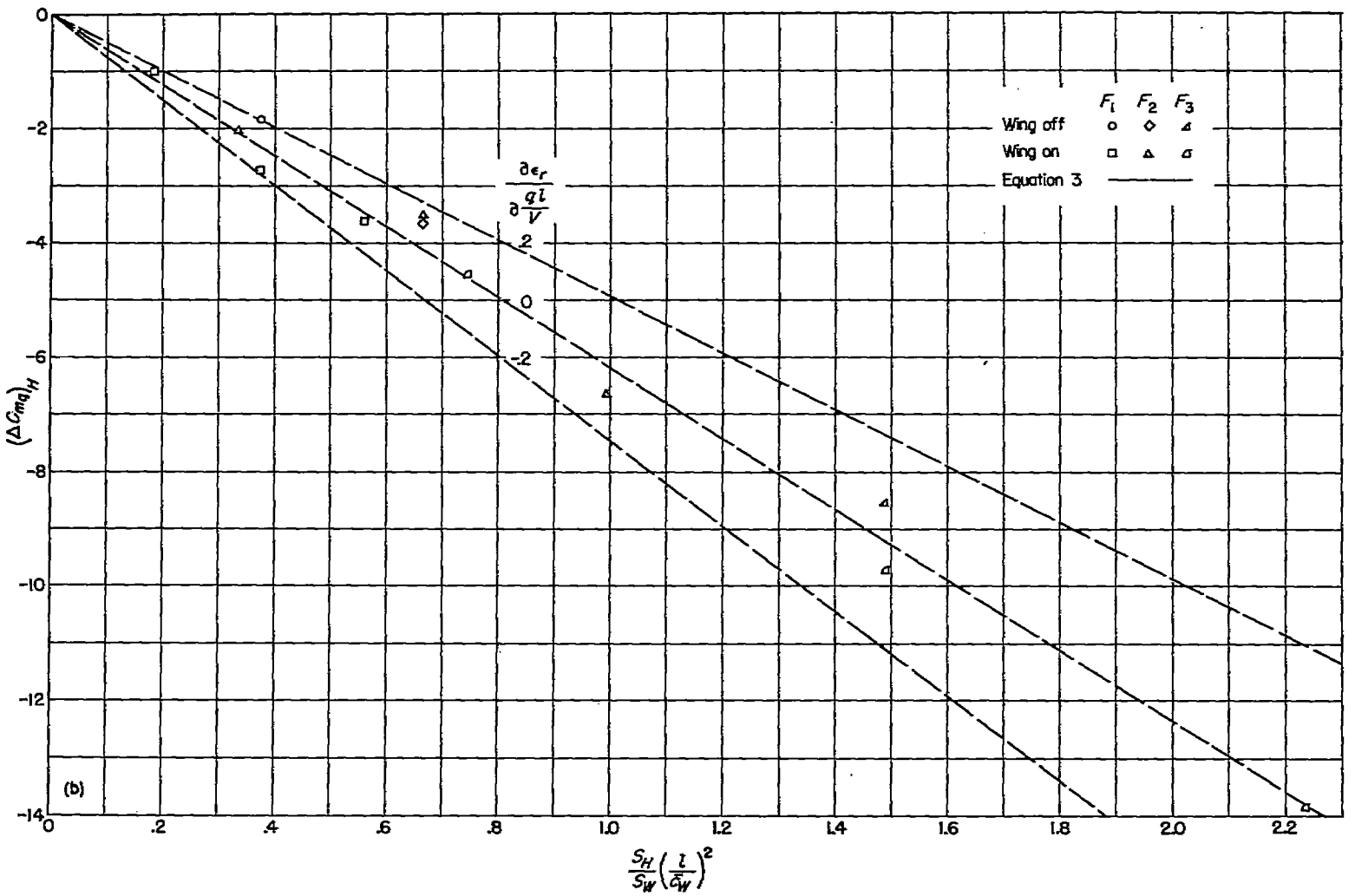

(b) Variation of $(\Delta C_{m_q})_H$ with $\frac{S_H}{S_W}\left(\frac{l}{\bar{c}_W}\right)^2$.

FIGURE 12.—Concluded.

parameter $\frac{\partial \epsilon_r}{\partial \frac{ql}{V}}$ which affects the damping in pitch is essentially zero for all tail positions; therefore, the standard methods of calculating the horizontal-tail contribution to C_{m_q} were found to be reliable for all horizontal-tail configurations tested. The position of the test values for the wing-on conditions relative to those for the wing-off conditions indicates, in fact, that the wing contributed a slightly negative value of $\frac{\partial \epsilon_r}{\partial \frac{ql}{V}}$; thus, an increase in the tail effectiveness for damping in pitch resulted.

A slight increase in tail effectiveness due to the presence of the wing would be expected from consideration of the unusual downwash pattern behind a swept wing in pitching flight. For a sweptback wing pitching about the aerodynamic center at zero angle of attack, the center part of the wing, which is forward of the aerodynamic center, is at an effective negative angle of attack and thereby induces an effective upwash at the horizontal tail. The tail, consequently, is at an effective higher angle of attack with the wing on than with the wing off. Since this effect increases with increasing pitching rotation, the wing will tend to increase the damping-in-pitch contribution obtained from the tail at low angles of attack. Some approximate computations were made to determine the upwash at the tail due to pitching flight, and the results indicated the same trend shown experimentally.

The data also show that, as indicated by equation (3), the contribution of the horizontal tail to the rotary damping in pitch varies linearly with tail area and with the square of tail length.

Although, at low angles of attack, the vertical position of the horizontal tail was not found to be significant for the steady-state rotary damping in pitch, it might be expected that the vertical position of the horizontal tail would influence the total damping of an airplane in a pitching oscillation. For a pitching oscillation, the total damping is determined by a combination of the rotary derivative C_{m_q}, which is considered herein, and the acceleration derivative $C_{m_{\dot{\alpha}}}$. The derivative $C_{m_{\dot{\alpha}}}$ is proportional to $\frac{\partial \epsilon}{\partial \alpha}$ (see reference (3)) and, therefore, should depend rather strongly on the location of the horizontal tail.

WING-FUSELAGE INTERFERENCE

The data obtained in the investigation of the horizontal-tail effect also make possible an evaluation of the interference increments $\Delta_1 C_{m_\alpha}$ and $\Delta_1 C_{m_q}$ which enter into the following

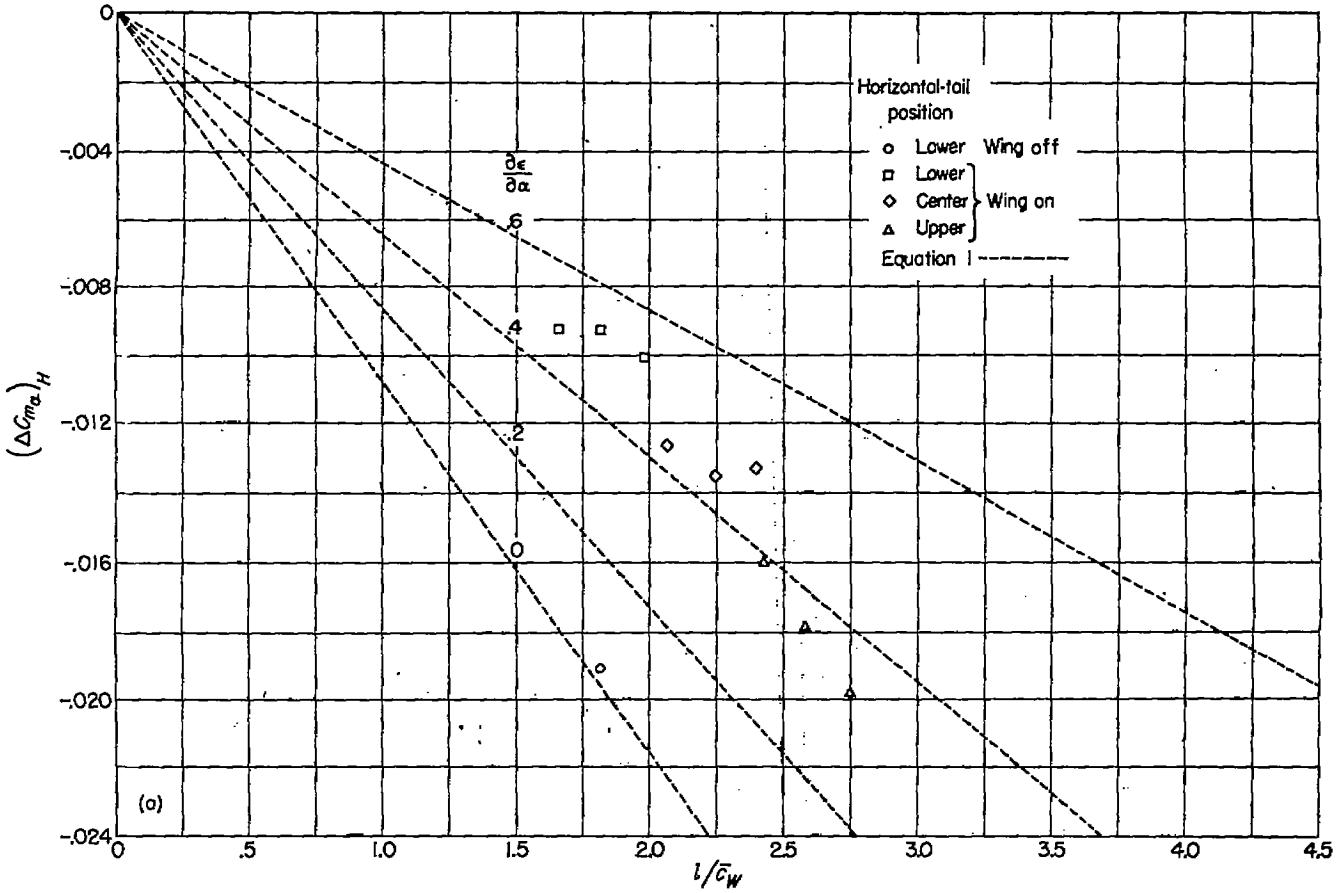

(a) Variation of $(\Delta C_{m_\alpha})_H$ with $\frac{l}{\bar{c}_W}$.

FIGURE 13.—Variation of the increment in static longitudinal stability and damping in pitch due to the horizontal tail with geometric parameters. Vertical position of the horizontal tail varied. Lift-curve slope of the horizontal tail was assumed to be 0.54. $\alpha = 0°$.

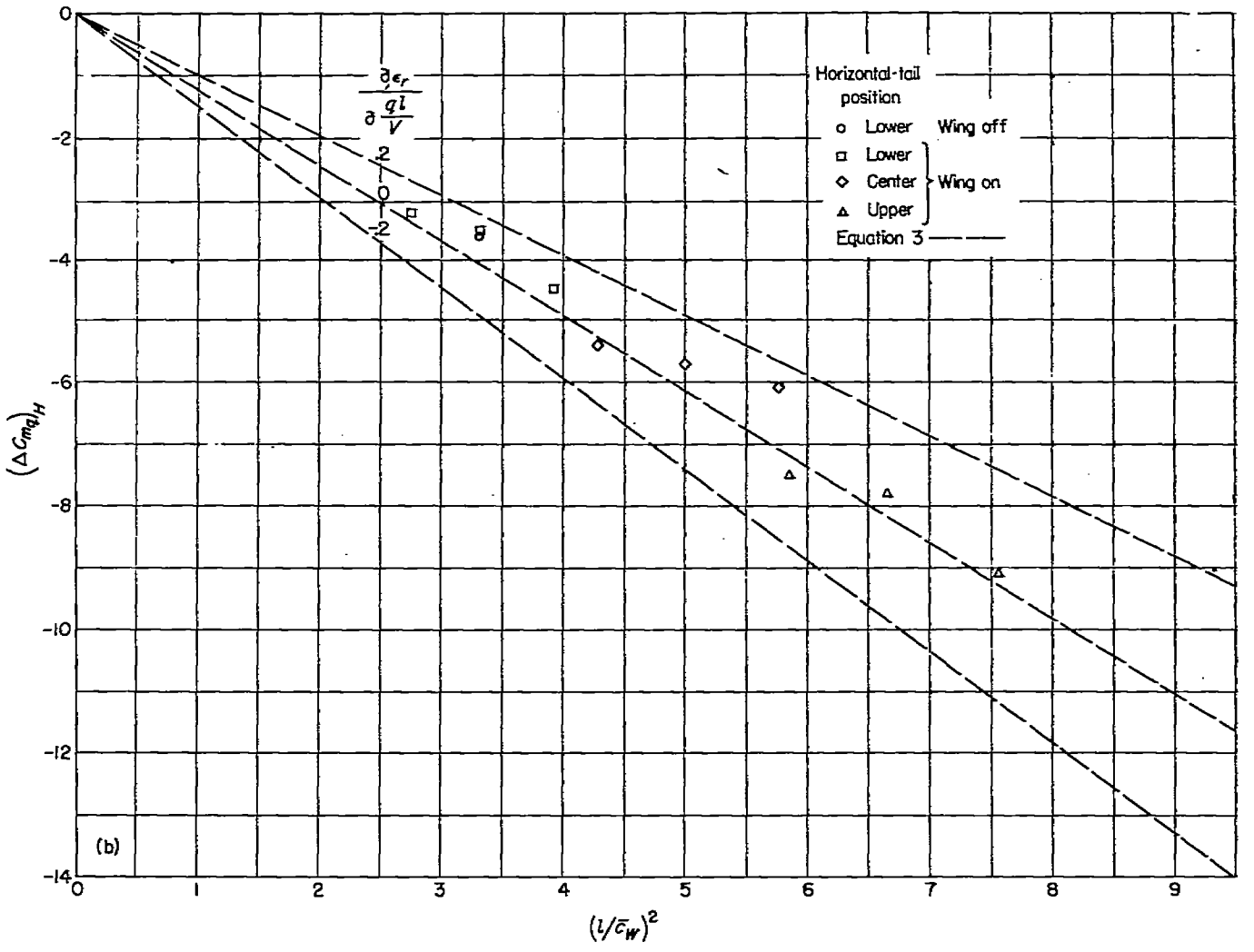

(b) Variation of $(\Delta C_{m_q})_H$ with $\left(\frac{l}{\bar{c}_W}\right)^2$.

FIGURE 13.—Concluded.

equations for total values of the static-longitudinal-stability and damping-in-pitch derivatives for complete airplane configurations:

$$(C_{m_\alpha})_{Total}=(C_{m_\alpha})_W+(C_{m_\alpha})_F+\Delta_1 C_{m_\alpha}+(\Delta C_{m_\alpha})_H$$

$$(C_{m_q})_{Total}=(C_{m_q})_W+(C_{m_q})_F+\Delta_1 C_{m_q}+(\Delta C_{m_q})_H$$

where $(\Delta C_{m_\alpha})_H$ and $(\Delta C_{m_q})_H$ are the values for the horizontal tail in the presence of the wing and fuselage. The values $\Delta_1 C_{m_\alpha}$ and $\Delta_1 C_{m_q}$ result from interference between the wing and fuselage (that is, $\Delta_1 C_{m_q}=(C_{m_q})_{W+F}-(C_{m_q})_W-(C_{m_q})_F$). The interference increments usually are assumed to apply to airplanes having configurations somewhat similar to that of the model used in evaluating the increments. The height of the wing relative to the fuselage center line usually has a significant effect on the magnitude of the interference increments. Since, for the present investigation, the wing was located on the fuselage center line, the results are considered applicable only to midwing or near midwing arrangements.

The increments are presented in figure 14 as functions of angle of attack. Within the accuracy of the determinations

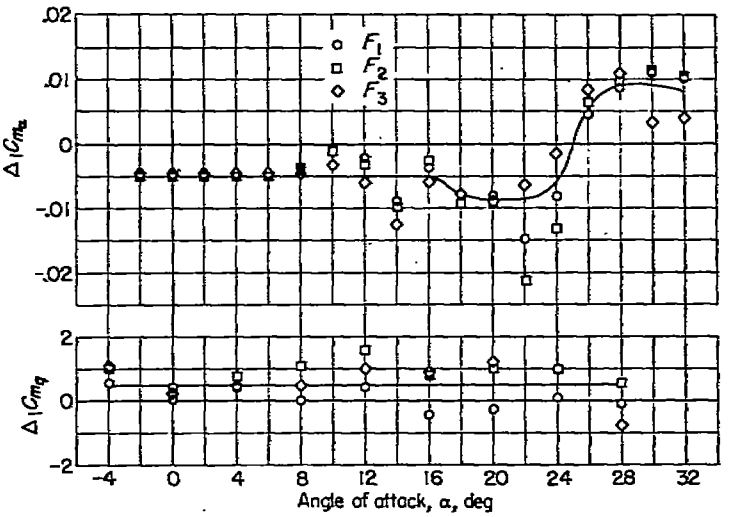

FIGURE 14.—Variation of wing-fuselage interference increments $\Delta_1 C_{m_\alpha}$ and $\Delta_1 C_{m_q}$ with angle of attack.

there appeared to be no consistent effect of fuselage length on either $\Delta_1 C_{m_\alpha}$ or $\Delta_1 C_{m_q}$ and, for the purposes for which these values were intended to be used, the use of a faired value to represent the effect of interference seems reasonable. The variation of $\Delta_1 C_{m_\alpha}$ with angle of attack is small below 16° and the average value tends to increase the stability. The variation of $\Delta_1 C_{m_q}$ with angle of attack is not appreciable over the entire angle-of-attack range and the average value tends to decrease the damping.

CONCLUSIONS

The results of an investigation to determine the effects of horizontal-tail size, tail length, and position on the static longitudinal stability and on the steady-state rotary damping in pitch of a complete model with wing and tail surfaces having the quarter-chord lines swept back 45° and an aspect ratio of 4 indicate the following conclusions:

(1) The contribution of the horizontal tail to static longitudinal stability and damping in pitch was in agreement with analytic considerations in that the contribution of the horizontal tail to static longitudinal stability was related directly to the tail size and length; whereas, its contribution to damping in pitch was related directly to tail size and the square of tail length.

(2) At low angles of attack, addition of the wing decreased the contribution of the horizontal tail to static longitudinal stability by about one-half to one-third, depending upon the vertical position of the tail relative to the wing; the contribution of the horizontal tail to the rotary damping in pitch, on the other hand, was almost unaffected by addition of the wing, regardless of the tail area or location.

(3) For configurations with the horizontal tail mounted along the fuselage center line, the static longitudinal stability was greater at angles of attack near the stall than at 0°; the longitudinal stability characteristics were impaired, however, by moving the horizontal tail upward. On the other hand, for configurations with the horizontal tail mounted along the fuselage center line, the rotary damping in pitch was less at angles of attack near the stall than at 0°, but the damping in pitch was generally increased by moving the tail upward.

(4) At an angle of attack of about 10°, the static longitudinal stability of the wing-fuselage combinations changed adversely. The magnitude of this change was slightly increased by the addition of tail area along the fuselage center line at the shortest tail length but was decreased by addition of area along the fuselage center line at the longest tail length.

LANGLEY AERONAUTICAL LABORATORY,
NATIONAL ADVISORY COMMITTEE FOR AERONAUTICS,
LANGLEY FIELD, VA., *April 1, 1952.*

REFERENCES

1. MacLachlan, Robert, and Letko, William: Correlation of Two Experimental Methods of Determining the Rolling Characteristics of Unswept Wings. NACA TN 1309, 1947.
2. Goodman, Alex, and Brewer, Jack D.: Investigation at Low Speeds of the Effect of Aspect Ratio and Sweep on Static and Yawing Stability Derivatives of Untapered Wings. NACA TN 1609, 1948.
3. Cowley, W. L., and Glauert, H.: The Effect of the Lag of the Downwash on the Longitudinal Stability of an Aeroplane and on the Rotary Derivative M_q. R. & M. No. 718, British A.R.C., 1921.
4. Jones, Robert T., and Fehlner, Leo F.: Transient Effects of the Wing Wake on the Horizontal Tail. NACA TN 771, 1940.
5. Brewer, Jack D., and Lichtenstein, Jacob H.: Effect of Horizontal Tail on Low-Speed Static Lateral Stability Characteristics of a Model Having 45° Sweptback Wing and Tail Surfaces. NACA TN 2010, 1950.
6. Queijo, M. J., and Wolhart, Walter D.: Experimental Investigation of the Effect of Vertical-Tail Size and Length and of Fuselage Shape and Length on the Static Lateral Stability Characteristics of a Model With 45° Sweptback Wing and Tail Surfaces. NACA Rep. 1049, 1951. (Supersedes NACA TN 2168.)
7. Munk, Max M.: The Aerodynamic Forces on Airship Hulls. NACA Rep. 184, 1924.
8. Purser, Paul E., Spearman, M. Leroy, and Bates, William R.: Preliminary Investigation at Low Speed of Downwash Characteristics of Small-Scale Sweptback Wings. NACA TN 1378, 1947.
9. Toll, Thomas A., and Queijo, M. J.: Approximate Relations and Charts for Low-Speed Stability Derivatives of Swept Wings. NACA TN 1581, 1948.